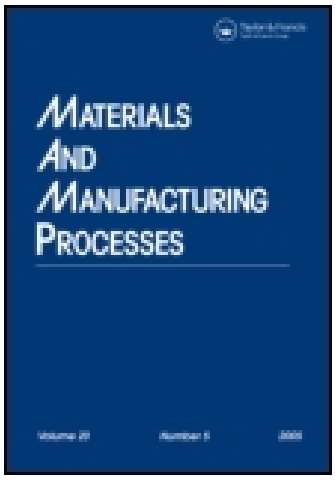

Materials and Manufacturing Processes
Publication details, including instructions for authors and subscription information:
http://www.tandfonline.com/loi/lmmp20

The Effect of Peak Power and Pulse Duration for Dissimilar Welding of Brass to Stainless Steel

Yang Li [a b], Shengsun Hu [a b] & Junqi Shen [a b]
[a] School of Materials Science and Engineering, Tianjin University, Tianjin, China
[b] Tianjin Key Laboratory of Advanced Joining Technology, Tianjin University, Tianjin, China
Accepted author version posted online: 18 Mar 2014.Published online: 18 Jul 2014.

To cite this article: Yang Li, Shengsun Hu & Junqi Shen (2014) The Effect of Peak Power and Pulse Duration for Dissimilar Welding of Brass to Stainless Steel, Materials and Manufacturing Processes, 29:8, 922-927, DOI: 10.1080/10426914.2014.901531

To link to this article: http://dx.doi.org/10.1080/10426914.2014.901531

Materials and Manufacturing Processes, 29: 922–927, 2014

ISSN: 1042-6914 print/1532-2475 online
DOI: 10.1080/10426914.2014.901531

Taylor & Francis
Taylor & Francis Group

The Effect of Peak Power and Pulse Duration for Dissimilar Welding of Brass to Stainless Steel

Yang Li[1,2], Shengsun Hu[1,2], and Junqi Shen[1,2]

[1]*School of Materials Science and Engineering, Tianjin University, Tianjin, China*
[2]*Tianjin Key Laboratory of Advanced Joining Technology, Tianjin University, Tianjin, China*

A pulsed Nd:YAG laser was used to weld overlap joint between H62 brass and 316L stainless steel in thermal conductivity welding mode. Effects of peak power and pulse duration were investigated under the condition of constant pulse energy. Optical microscopy (OM), scanning electron microscope, and X-ray diffraction were used to analyze the microstructure, defects, and intermetallic phases in the interface, respectively. Microhardness test and tensile test were carried out to identify the mechanical property on the welded joints. The results showed that the microstructure, penetration-to-width ratio (φ), and mechanical properties were affected by the combined effects of peak power and pulse duration when the pulse energy was constant. When the magnitude of the peak power equals to 1846 W, both of penetration-to-width ratio and microhardness in the welded joints stayed to a minimum value. But if the magnitude of the peak power is less than 1846 W, the welded joint has the fewer defects, superior microstructure, and mechanical properties while comparing with the greater peak power.

Keywords Brass; Dissimilar; Laser; Mechanical; Property; Stainless; Steel; Welding.

Introduction

In recent years, welded components needed superior performance and stricter operating requirement based on the industrial development and the technological progress. Therefore, only one kind of metal welding has been not suitable for the complex function in engineering applications. The dissimilar material welding, as a promising approach to technology, has been received extensive attention and made amazing progress in the petroleum chemical industry and aerospace fields [1, 2]. Owing to the advantages of high thermal conductivity, superior mechanical strength, and high corrosion resistance, a welded joint formed between stainless steel and copper alloy was regarded as the most significant progress in dissimilar joining applied in the aerospace, machinery, metallurgical, and refrigeration industries.

Currently, there are several dominating welding methods of stainless steel and copper alloy such as ultrasonic welding, friction stir welding, resistance welding, electron beam welding, and laser welding. For the reason of the obvious difference in melting point, thermal conductivity, and coefficient of linear expansion of the two metals, it is therefore difficult to form a welded joint between stainless steel and copper alloy. Hence, achieving the defect-free stainless steel to copper alloy dissimilar joint using the conventional methods mentioned above seems impossible. Electorn beam welding was often used in manufacturing the dissimilar joint due to the high power density heating sources, high speed, and narrow heat-affected zone [3–5]. However, electron beam welding needs vacuum conditions and demagnetization before welding, making it even harder. By comparing with the electron beam welding, the laser welding not only inherits the advantages (high power density heating sources, high speed, and limited heat-affected zone) of electron beam welding, but also uses shielding gas replace vacuum condition to solve the defects of electron beam welding. Hence, laser welding [6–10] is considered as a promising method to join copper-base alloy and stainless steel at present.

In this paper, the influence of pulse duration and peak power under the condition of constant pulse energy using a Nd:YAG pulsed laser beam were investigated. The objective of this investigation aims at the optimal process parameters on microstructure and mechanical properties in H62 brass to 316L stainless steel welding by Nd:YAG pulsed laser.

Experimental procedures

Materials

The materials used in the pulsed laser experiments were 316L stainless steel and H62 brass. The thickness of 316L stainless steel and H62 brass sheets was 0.9 mm and 0.4 mm, respectively. The dimension of the 316L stainless steel sheets for the welding was 100 mm × 20 mm × 0.9 mm (length × width × thickness). The dimension of the H62 brass sheets for the welding was 100 mm × 20 mm × 0.4 mm (length × width × thickness). Brass-on-stainless steel overlap configuration was used in this study, as shown in Fig. 1.

The most important thermophysical properties of the two materials are listed in Table 1. Apparently, the physical

Received January 6, 2014; Accepted February 19, 2014

Address correspondence to Junqi Shen, Room C0804, Building 25, School of Materials Science and Engineering, Tianjin University, Weijin Road 92, Nankai District, Tianjin 300072, People's Republic of China; E-mail: shenjunqi@tju.edu.cn

Color versions of one or more of the figures in the article can be found online at www.tandfonline.com/lmmp.

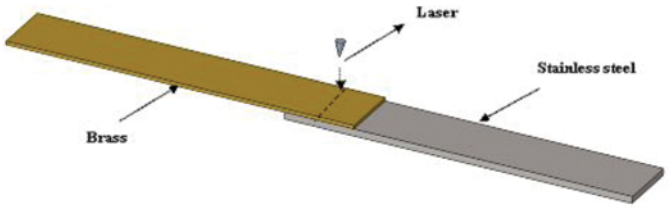

FIGURE 1.—The overlap configuration.

TABLE 1.—Thermophysical properties of steel and brass at room temperature [11].

Metal	Melting point (°C)	Resistivity ($\Omega\,mm^2/m$)	Density (g/cm^3)	Conductivity (W/m°C)	Heat capacity (J/kg K)	coefficient of linear expansion
Steel	1371	0.71	7.98	14 ~ 21	485	16.0
Brass	934	0.071	8.5	108.9	390	20.6

properties including density melting temperature, thermal conductivity, and linear expansion coefficient of brass and steel are strikingly different. These differences can be expected to increase the difficulty of welding. Meanwhile, the heat cracking and residual stress are difficult to avoid.

Processing Parameters

A pulsed Nd:YAG laser system (JK2003SM) with laser beam diameter of 0.6 mm was used in this study. When comes to the laser parameters, the maximum output power was 4 kW, the available range were 0–40 J for pulse energy, 100–1000 s^{-1} for repetition rate, and 1×10^{-3}–1×10^{-2} s for pulse duration. The output waveform of this laser was standard square shape pulses. The pure argon, as the shielding gas, was used during the welding operation with a flow rate of 20 L/min.

Prior to welding, joining surfaces of the H62 brass and 316L stainless steel blanks were polished with abrasive paper of grade 800 to remove the oxide film on the surface of the metals in the welding process, and then degreased with acetone. For each combination of parameter of the system, the experiments were replicated for three times. Then microstructures and the composition of the welded joint were observed using optical microscopy and X-ray diffraction, respectively. Once the optical microscopic examination has finished, the microhardness values of the welded joints were conducted with a 100 g load by using MHV2000 Vickers microhardness tester (Shanghai Material Testing Machine Factory, Shanghai, China). Finally, the tensile shear force value was carried out by using CSS-44100 universal testing machine (Changchun Research Institute for Testing Machines), and the fracture surface morphology was observed by scanning electron microscopy.

Figure 2 is a schematic diagram of the pulse waveform of laser welding used in the experiments. This is presented by the following equation:

$$P_a = \frac{P_P t_P + P_b t_b}{t_P + t_b} \tag{1}$$

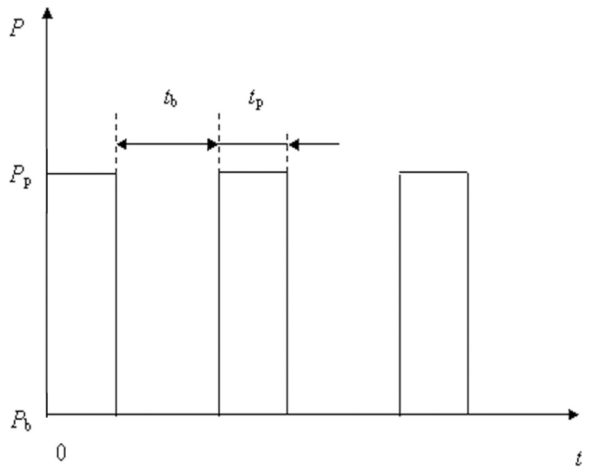

FIGURE 2.—Pulse waveform of laser welding.

where P_a is the average power, P_p is the peak power, P_b is the background power, t_p is the peak time, and t_b is the background time. In our investigation, P_b takes the value of 0 W in particularly.

When $P_b = 0$ W, the single pulse energy (E_S) would be calculated using the equation:

$$E_S = P_P \times t_p \tag{2}$$

where P_p is the peak power and t_p is the pulse duration. When single pulse energy (E_S) is a constant, both the peak power (P_p) and pulse duration (t_p) affect the microstructure and mechanical properties of the welded joints as shown in the Eq. (2). In this paper, the effects of peak power and pulse duration in constant pulse energy were investigated.

The power density (ρ) was calculated using the equation:

$$\rho = \frac{4P_P}{\pi d^2} \tag{3}$$

ehere P_P is the peak power and d is the spot diameter.

The penetration-to-width ratio (φ) was calculated by using the equation:

$$\varphi = H/B \tag{4}$$

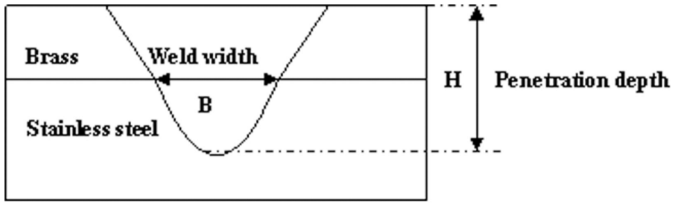

FIGURE 3.—Penetration depth-to-weld width ratio.

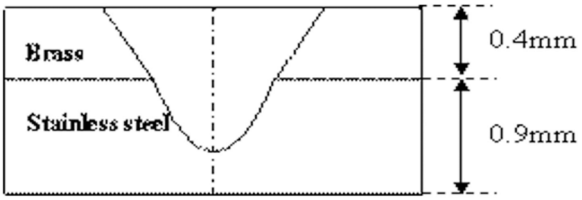

FIGURE 4.—Microhardness distribution on cross section.

where H is the penetration depth and B is the weld width, as shown in Fig. 3. It would form a narrow and deep welded joint when φ has a higher value. The test line of the microhardness in the welded joint was along the dash line marked from brass to stainless steel in Fig. 4.

RESULTS AND DISCUSSION

Macromorphological Characterization

The weld penetration depth and weld width with peak power and pulse duration under the condition of constant pulse energy were investigated. Experimental parameters are shown in Table 2 and the penetration depth and weld width value of Test No. 1 to No. 9 are shown in Fig. 5.

Figure 5 shows the various penetration depths and weld widths in different parameters of test Nos. 1–9 (Table 2). As can be seen from Fig. 5, penetration depth value of Test No. 1 is less than Test No. 2 and Test No. 3. The reason may be that the peak power of Test No. 1 is too low which leads to insufficient intermixing of the two materials in the welded joint. Hence, the penetration depth value of Test No. 1 is less than Test No. 2. However, as for test Nos. 2–9, penetration depth has the minimum value of 805 while peak power is 1846 W. On the other hand, the weld width value has no obvious change for all the test samples, as shown in Fig. 5.

Figure 6 shows the variation of penetration-to-width ratio on the basis of peak power according to Table 2. The curve changes in the "V" shape from Test Nos. 2–9. Meanwhile, the penetration-to-width ratio of Test No. 1, No. 2, and No. 3 is close to each other. The minimum value of penetration-to-width ratio is 1.320, when peak power is 1846 W, as shown in Fig. 6.

TABLE 2.—Variation of peak power and pulse duration in constant pulse energy.

Test no.	Average power (W)	Pulse frequency (s^{-1})	Velocity (mm/s)	Power density (W/cm^2)	Peak power (W)	Pulse duration (s)
1	1200	200	13	4.47×10^5	1263	4.75×10^{-3}
2	1200	200	13	4.75×10^5	1341	4.5×10^{-3}
3	1200	200	13	5.00×10^5	1412	4.25×10^{-3}
4	1200	200	13	5.32×10^5	1500	4×10^{-3}
5	1200	200	13	5.67×10^5	1600	3.75×10^{-3}
6	1200	200	13	6.07×10^5	1714	3.5×10^{-3}
7	1200	200	13	6.53×10^5	1846	3.25×10^{-3}
8	1200	200	13	7.71×10^5	2182	2.75×10^{-3}
9	1200	200	13	9.44×10^5	2667	2.25×10^{-3}

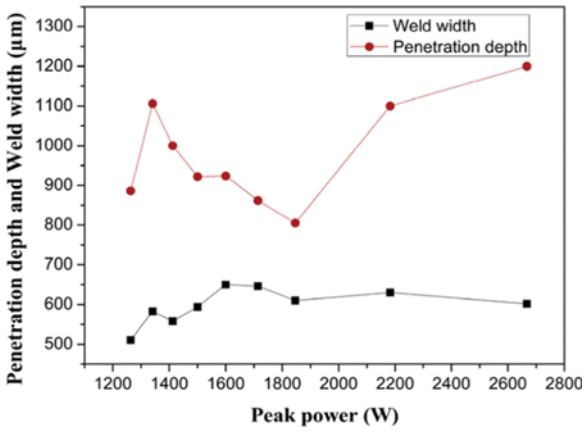

FIGURE 5.—Penetration depth and weld width.

Power density (ρ) mainly influences the heating velocity of the material's surface. When the peak power is greater than 1846 W, the laser energy is more intensive with the increasing of peak power. And the intensive laser energy will result in higher rising velocity of the materials and higher penetration-to-width ratio of the welded joints.

In the case of the peak power less than 1846 W, the penetration-to-width ratio gets smaller with a greater peak power. This is because that the materials have the short heating time when the peak power is less than 1846 W. And the heating time is determined by the pulse duration. It speculates that, when the average power and pulse frequency were constant, peak power and pulse duration both influence the penetration-to-width ratio. When peak power is greater than 1846 W, peak power was the main affecting factor of the penetration-to-width ratio. However, when peak power is less than 1846 W, pulse duration was the main affecting factor of the penetration-to-width ratio.

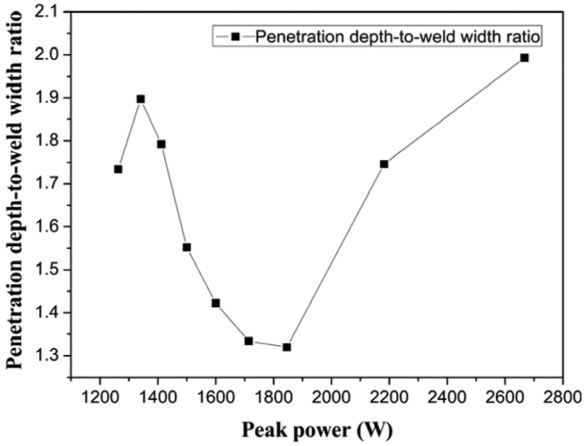

FIGURE 6.—The penetration-to-width ratio (φ).

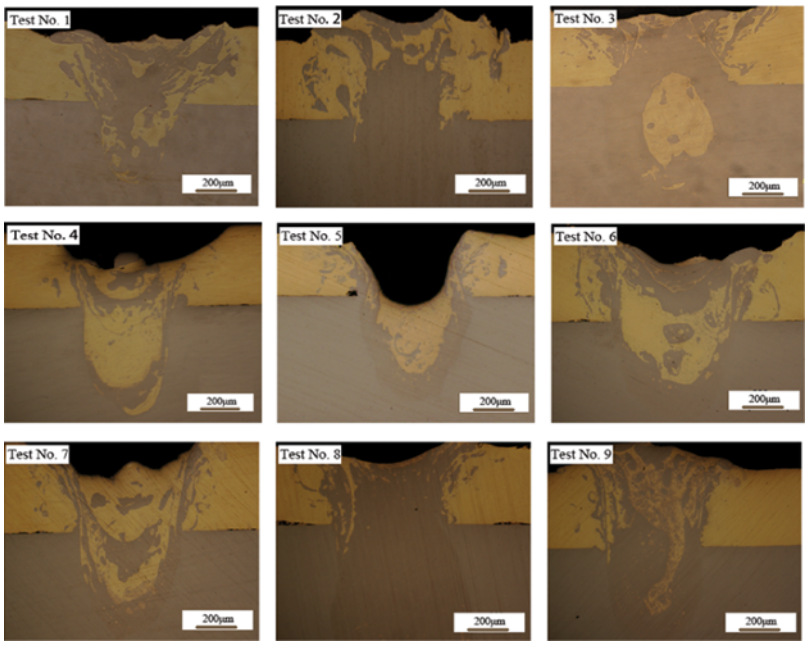

FIGURE 7.—Cross section of brass–stainless steel joints.

Metallurgical Characterization

Figure 7 are the optical micrographs, which reveals the cross section of brass–stainless steel joints according to test Nos. 1–9 in Table 2. Regarding Test Nos. 4–7, due to the low melting point element zinc evaporation, defect of surface depression appeared in the welded joint. For Test Nos. 1–3, due to the low peak power and low temperature, the evaporation capacity of zinc was low. For Test Nos. 8–9, due to the short heating time, zinc has no time to evaporate. In other words, when the peak power is greater than 2182 W (Test No. 8 and Test No. 9) or less than 1412 W (Test Nos. 1–3), the welded joint has the superior surface quality. Moreover, the microstructure of the welded joints in Fig. 7 and the power density value in Table 2 show that the thermal conductivity welding occured at the condition of these welding parameters.

Meanwhile, there are no intermetallic phases in the interface, as shown in Fig. 8. The reason is that atomic radii, lattice type, and lattice constant of copper were close to those of Fe at high temperature (see ref. [10]). They could be unlimited solid solution in liquid phase and limited solid solution in solid phase with difficulty to forming intermetallic compounds.

To examine the detailed information of the joints, the cross-sectional micrographs of the specimens were

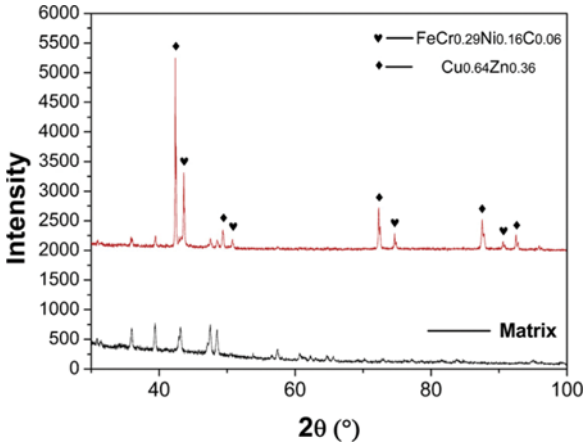

FIGURE 8.—X-ray diffraction results of the welded joint.

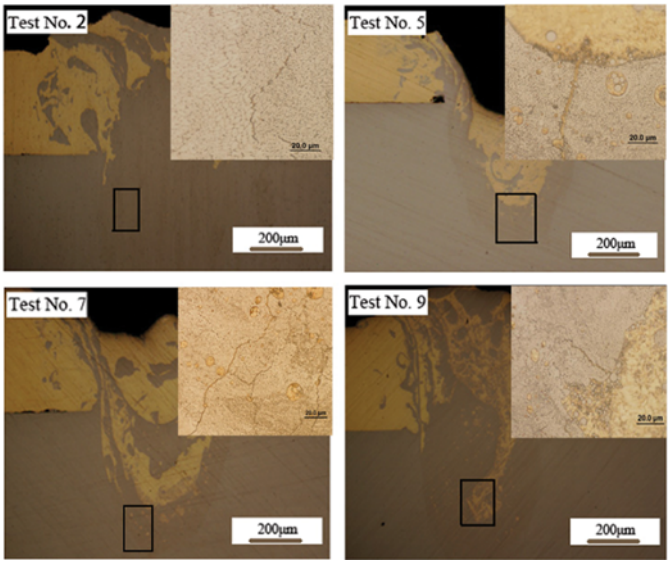

FIGURE 9.—The cracks in the welded joint.

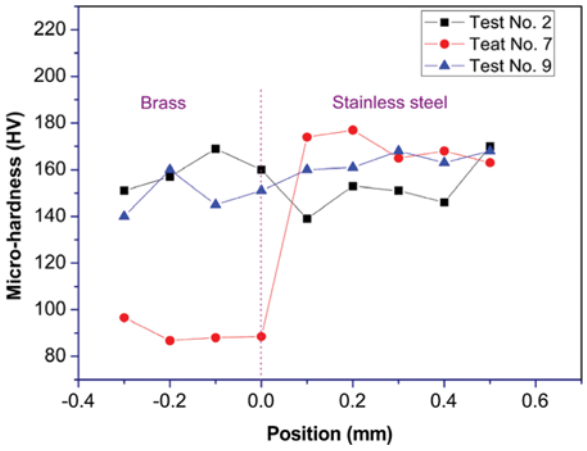

FIGURE 10.—Variation of hardness at the welded joint of Test Nos. 2, 7 and 9.

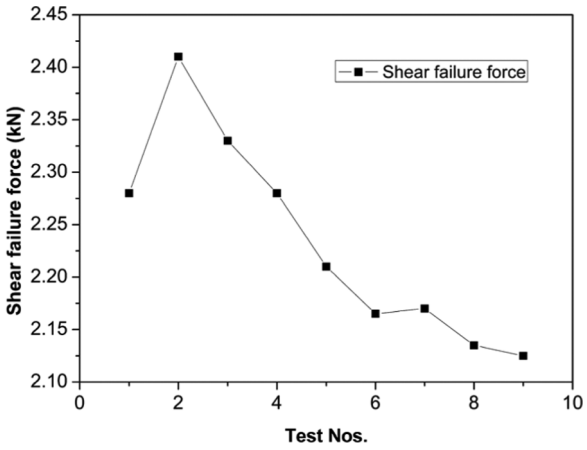

FIGURE 11.—The load of all Test Nos.

etched with 10 g $FeCl_3 + 20$ mL $HCl + 40$ mL H_2O. And then, it obtained more information about defects in the welded joints. There were a few cracks existing in the interface between brass and stainless steel in the welded joint. The main defect in the interface of brass and stainless steel was penetrating cracks, as shown in Fig. 9. Two main factors leading to the cracks in the mixed zone of stainless steel and brass could be summarized as follows: first, there was an osmosis of brass to stainless steel, so liquid copper could infiltrate to the stainless steel; second, the brass has a larger linear expansion coefficient and a larger cooling shrinkage in cooling, which would produce residual tensile stress and stress concentration at the time of crystallization in the molten pool. This was also an important reason of the crack formation.

Moreover, as it was seen, cracks increases by increasing peak power in Fig. 9. The reason was that as the peak power increases, heating and cooling rates in the interface also increase dramatically. The increasing heating and cooling rates resulted in greater residual tensile stress and stress concentration, which bring out cracks in the welded joint easily.

Microhardness of the Welded Joint

The test line of the microhardness in the welded joint was along the dash line marked from brass to stainless steel in Fig. 4. The results are the average value of testing for three times, as shown in Fig. 10. Microhardness in the weld of sample 2 and sample 9 are higher than that of sample 7. For sample 2 and sample 9, welded joint microhardness approximates base metal stainless steel because of the penetrated stainless steel in the welded joint. However, for sample 7, the microhardness decreased slightly in the welded joint because of the inadequately mixing of brass and stainless steel in welded joint.

Tensile Stress

Figure 11 presents the respective shear failure force on each of the specimens. The results are the average value of three samples. Obviously, the shear failure force of Test No. 2 is significantly higher than the others. The increase in the peak power is likely to result in stress concentration, which will bring out low shear failure force due to the high heating and cooling velocity. Hence, with the increasing of peak power, the shear failure force gets lower for Test Nos. 2–9. However, the peak power of Test No. 1 is too low, which leads to insufficient intermixing of the two materials in the welded joint; therefore, the shear failure force of Test No. 1 is lower than that of Test No. 2.

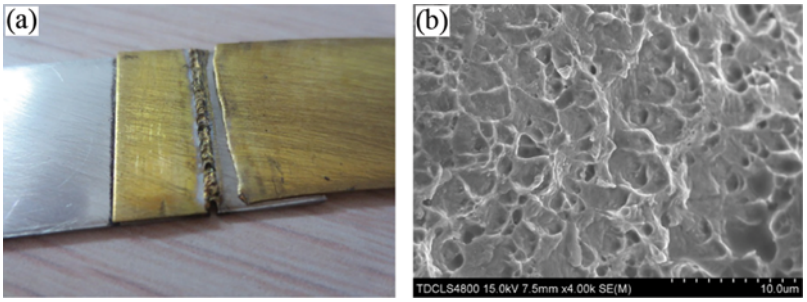

FIGURE 12.—Fracture surface morphology of welded joint.

From the shear failure force tests, fracture occurred in the fusion zone of the welded joint, as shown in Fig. 12(a). The fracture surface morphology of welded joint is shown in Fig. 12(b). There are numerous dimples that can be found on the fracture surface in all welded joint. The dimple indicating that the fracture mode of the welded joint is ductile fracture. As a result, the ductile fracture reasons the failures of all the welded joints.

Conclusions

The effects of two different series process parameters on H62 brass–316L stainless steel joints produced by pulsed Nd:YAG laser welding have been analyzed. Following are the conclusions obtained from the present study:

1. Peak power and pulse duration both influence the penetration-to-width ratio and the microhardness on the welded joint under the condition of constant pulse energy. The penetration-to-width ratio has a minimum value when the peak power was 1846 W. Meanwhile, the microhardness value was minimal when the penetration-to-width ratio was minimal.
2. Increasing the peak power will increase the cracks in the interface under the condition of constant pulse energy. However, the cracks will decrease the shear failure force of the joints.
3. A peak power of 1341 W and a pulse duration of 4.5×10^{-3} s are the optimized parameters when the other welding parameters are fixed. Superior penetration-to-width ratio, high quality surface, and superior mechanical properties (microhardness and shear failure force) can be obtained with the optimized parameters.

Funding

The authors gratefully acknowledge support from the National Natural Science Foundation of China (Grant No. 50975195).

References

1. Luo, J.; Wang, X.M.; Liu, D.J.; Li, F.; Xiang, J.F. Inertia radial friction welding joint of large size H90 Brass/D60 steel dissimilar metals. *Materials and Manufacturing Processes* **2012**, *27* (9), 930–935.
2. Laser lap joining of dissimilar materials: a review of factors affecting joint strength. *Materials and Manufacturing Processes* **2013**, *28* (8), 857–871.
3. Magnabosco, I.; Ferro, P.; Bonillo, F.; Arnberg, L. An investigation of fusion zone microstructures in electron beam welding of copper–stainless steel. *Materials Science and Engineering A* **2006**, *424*, 163–173.
4. Tosto, S.; Nenci, F.; Hu, J.D.; Corniani, F.G.; Pierdominici, F. Microstructure of copper–AISI type 304L electron beam welded alloy. *Materials Science and Technology* **2003**, *19*, 519–522.
5. Gao, M.; Mei, S.W.; Wang, Z.M.; Li, X.Y.; Zeng, X.Y. Characterisation of laser welded dissimilar Ti/steel joint using Mg interlayer. *Science and Technology of Welding and Joining* **2012**, *17*, 269–276.
6. Mourada, A.-H.I.; Khourshid, A.; Sharef, T. Gas tungsten arc and laser beam welding processes effects on duplex stainless steel 2205 properties. *Materials Science and Engineering A* **2012**, *549*, 105–113.
7. Mai, T.A.; Spowage, A.C. Characterisation of dissimilar joints in laser welding of steel-kovar, copper-steel and copper-aluminum. *Material Science and Engineering A* **2004**, *374*, 224–233.
8. Wu, D.J.; Ma, G.Y.; Niu, F.Y.; Guo, D.M. Pulsed laser welding of hastelloy C-276: high-temperature mechanical properties and microstructure. *Materials and Manufacturing Processes* **2013**, *28* (5), 524–528.
9. Yao, C.W.; Yao, B.S.; Zhang, X.Ch.; Huang, J.; Fu, J.; Wu, Y.X. Interface microstructure and mechanical properties of laser welding copper-steel dissimilar joint. *Optics and Lasers in Engineering* **2009**, *47*, 807–814.
10. Shen, J.; Wen, L.B.; Li, Y.; Min, D. Effects of welding speed on the microstructures and mechanical properties of laser welded AZ61 magnesium alloy joints. *Materials Science and Engineering A* **2013**, *578*, 303–309.
11. Zhou, Z.F.; Zhang, W.Y. *Welding Metallurgy and Metal Weldability*; China Machine Press: Beijing, China, 1987.